

Prewavy instability-originated dielectric chevrons of electroconvection in nematic liquid crystals

Masato Shiomi¹, E-Joon Choi², and Jong-Hoon Huh¹

¹*Department of Physics and Information Technology, Faculty of Computer Science and Systems Engineering, Kyushu Institute of Technology, Fukuoka 820-8502, Japan*

²*Department of Polymer Science and Engineering, Kumoh National Institute of Technology, Gumi, Gyungbuk 730-701, Korea*

 (Received 3 August 2020; revised 30 September 2020; accepted 7 October 2020; published 26 October 2020)

This paper reports the pattern formation and evolution in a high-frequency dielectric regime observed in the AC-driven electroconvection of nematic liquid crystals (NLCs). It is determined that prewavy (PW) instability is essential for the formation and evolution. Specifically, in a twisted-aligned NLC cell, we observe a unique pattern that is comparable to the dielectric chevrons (DCVs) typically observed in a conventional planarly aligned pattern. It is determined to be a combined PW pattern with dielectric normal rolls (DNRs). Moreover, the power indices (α_{PW} , α_{DNR} , and α_{DCV}) are determined from the frequency-dependent thresholds ($V_{th} \propto f^\alpha$) of PW, DNR, and DCV. By taking into account the appearance of PW and the different power indices, the pattern evolution scenarios for DCV are proposed, which can well explain the previous experimental results. Specifically, the PW-originated DCV2 clearly differs from the defect-mediated DCV1, which is known as a typical pattern evolution.

DOI: [10.1103/PhysRevE.102.042704](https://doi.org/10.1103/PhysRevE.102.042704)

I. INTRODUCTION

For the past five decades, AC-driven electroconvection (EC) in nematic liquid crystals (NLCs) has been extensively investigated to understand the pattern formation in nonequilibrium dissipative systems [1,2]; it provides us a wide variety of patterns owing to the anisotropic properties of NLCs and controllable symmetries of the boundary conditions [2]. In general, EC is addressed in two typical regimes depending on the applied frequency f —the low-frequency conduction regime ($f < f_c$) and the high-frequency dielectric regime ($f > f_c$)—which are sharply differentiated by a characteristic cutoff frequency $f_c = (\xi^2 - 1)^{1/2} / 2\pi\tau_\sigma$. Here, $\xi^2 = (1 - \sigma_\perp \varepsilon_{//} / \sigma_{//} \varepsilon_\perp) (1 + \alpha_2 \varepsilon_{//} / \eta_1 \varepsilon_a) (\sim 1.7-3.5)$ and $\tau_\sigma = \varepsilon_0 \varepsilon_\perp / \sigma_\perp$ ($\sim 10^{-3}-10^{-2}$ s), respectively, denote the anisotropy parameter and the charge relaxation time, including viscous properties (α_2 and η_1), dielectric constants and anisotropy ($\varepsilon_a = \varepsilon_{//} - \varepsilon_\perp$), and electric conductivity ($\sigma_{//}$ and σ_\perp) [3–5]. It is known that Williams domains (WDs) and dielectric chevrons (DCVs) are typical EC for $f < f_c$ and $f > f_c$, respectively [5,6]; owing to the Carr-Helfrich mechanism, including the torque balance of the director and the Navier-Stokes equation for an anisotropic fluid (i.e., NLC), a WD is determined to be a stationary director field and has oscillating charge distributions, whereas a DCV is characterized by stationary charge distributions and oscillating director fields [5–7]. However, it has been clearly determined that a different typical instability exists, called the prewavy (PW) or wide domains [with a much larger wavelength $\lambda_{PW} (\sim 4d)$ than $\lambda_{WD} (\sim d)$ of a WD] [4,8–11]; more importantly, it straddles both regimes [2,5,9–11]. However, despite the important role of PW in pattern formation and evolution, its theoretical understanding remains poor [2,4,5,11].

In general, EC is induced by applying an electric field $\mathbf{E}(t) = (\sqrt{2}V/d) \cos(2\pi ft) \hat{\mathbf{z}}$ across an NLC layer (typically, thickness $d = 10-100 \mu\text{m}$) between two parallel electrodes with the initial director $\mathbf{n}_0 = (1, 0, 0)$. PW is known to be a background pattern of EC, which is characterized by clockwise- and counterclockwise-twisted domains of the director field [8,11]. Thus, it can be clearly distinguished from a typical EC (i.e., WD) with periodic splay-bend domains of the director field [5]. Accordingly, defect-free chevrons (DFCs) are observed for $f < f_c$, which result from the combination of a WD and PW [9–11]. Intuitively, when PW appears for $f > f_c$, a pattern combination (i.e., a dielectric pattern and PW) is also expected; however, PW has been rarely considered as the background pattern of EC in this regime because it has been examined independently in many studies [4,5,8,12]; moreover, pure PW has been observed in bent-core NLCs [13,14] and dimeric NLCs with a short-range smectic-C order [15]. On the other hand, a DCV is known to evolve from dielectric normal rolls (DNRs) through a small increase in V , independent of PW [12,16,17]. Although the striped domains (SDs) of a DCV provide almost the same director field for PW [12,16,17], they have been considered as a result of secondary instability causing twist modulations of the director field owing to the periodic defect ordering along the direction of a DNR (i.e., $\mathbf{k}_{SD} // \mathbf{k}_{DNR} // \mathbf{n}_0$) [16–18]. In this study, the main questions include whether PW relates to the formation of a DCV and what happens if the combination is realized; moreover, we examine how to distinguish the two types of twisted SDs that originate from PW and a DCV. Consequently, two types of DCV are presented; the present PW-originated DCV can be distinguished from the conventional DNR-developed DCV. Furthermore, the PW-originated model for chevrons can be compared with previous models such as the defect-mediated model [18], mode-coupling model [19], and beating

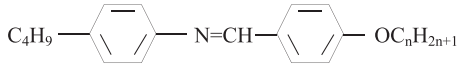


FIG. 1. Nematic liquid crystals (NLCs) used in this study. $n = 1$ and $n = 2$ indicate *p*-methoxybenzylidene-*p*-*n*-butylaniline (MBBA) and *p*-ethoxybenzylidene-*p*-*n*-butylaniline (EBBA), respectively.

model [20]; all models were developed to explain the herringbone structure characterized by two distinguishable wave vectors, although their approaches were quite different from one another.

This study aims to elucidate the pattern formation and evolution of EC in a dielectric regime ($f > f_c$). In Sec. II, the prepared cells and experimental methods are described. In Secs. III A and III B, two types of DCV are described by using optical patterns and threshold voltages. In particular, pure PW and PW combined with a DNR (or DCV) are examined in terms of the f -dependent thresholds; thus, the power indices (i.e., α_{DCV} and α_{PW} of $V_{\text{th}} \propto f^\alpha$) are determined and compared to $\alpha_{\text{DNR}} = 0.5$ (i.e., $V_{\text{th}} \propto f^{1/2}$), which is well understood [5,12]. In Secs. III C and III D, considering the thresholds and their power indices, possible scenarios on the formation of chevrons are suggested, and confirmed experimentally. Our findings aid in explaining the previous experimental results in which some incongruous points exist; for example, a DCV was determined by following a DNR [12–14] or through a direct transition from the rest state (without a DNR) [4,8,12,21]. In Sec. IV, the mechanism of PW is mentioned with a similar instability (i.e., inertia mode) [5,22], and previous different models for chevrons are compared and discussed with the present PW-originated model.

II. EXPERIMENT

In this work, two homolog compounds, *p*-methoxybenzylidene-*p*-*n*-butylaniline (MBBA) and *p*-ethoxybenzylidene-*p*-*n*-butylaniline (EBBA) are chosen

(Fig. 1), because binary mixtures of homologous series may have a eutectic point composition. This can lead to the formation of a nematic phase over a wide temperature range, and provide a broad frequency range for the experimental study on the dielectric region of EC ($> f_c$) [23]. To examine the EC patterns, their mixing rate-controlled sample cells are prepared (Table I).

In addition, two types of sample cells with different initial directors are prepared: one is called P-type (Cell1–8) with $\mathbf{n}_0 = (1, 0, 0)$ at $z = 0$ and $z = d$, and the other is T-type (Cell9–11) with $\mathbf{n}_0 = (1, 0, 0)$ at $z = 0$ and $\mathbf{n}_0 = (0, 1, 0)$ at $z = d$. The former has homogeneous directors along the z axis, whereas the latter has twisted directors along the z axis. The standard shadowgraph method is used for optical observations and measurements [4]. According to the requirements, a polarizer (P), an analyzer (A), and a quarter-wave plate (Q) are used, which are parallel, perpendicular, and $\pi/4$ to the x axis, respectively. Accordingly, the light propagates successively along the route: light source $\rightarrow P \rightarrow \text{NLC} \rightarrow Q \rightarrow A \rightarrow$ camera lens; this optical condition is referred to as PQA in this paper. If the A in the route is parallel set to the P , this is referred to as PQP. In particular, the optical conditions (PQA and PQP) can provide distinguishable clockwise- and counterclockwise-twisted domains [17,24]; the details of the experiment have been described in our recent paper [24].

III. RESULTS AND DISCUSSION

A. Two types of chevrons in the dielectric regime

First, typical PW, DFC, DNR, and DCV are observed in P-type cells, as shown in Fig. 2. For the PQA condition, clockwise- and counterclockwise-twisted domains are clearly distinguishable in pure PW [Fig. 2(a)], as well as in the DFC [Fig. 2(b)], for $f < f_c$, which must be a combination of WD and PW above the threshold $V_{\text{WD}} (> V_{\text{PW}})$ [9–11]; thus, the DFC is not equivalent to the DCV. Usually, the wave vector \mathbf{k}_{PW} of (pure) PW is parallel to

TABLE I. Properties of sample cells used in this study; all sample cells were prepared using commercial cells (E.H.C. Ltd., Japan).

Cell names	Alignment types ^a	Rate of NLCs (wt. %) ^b	Thickness $d(\mu\text{m}) \pm 5\%$	Conductivity $\sigma(\Omega^{-1} \text{m}^{-1})^c$	Dielectric constant ^c	Cutoff frequency $f_c^*(\text{Hz})^c$	$T_c(^{\circ}\text{C}) \pm 1^{\circ}\text{C}$
Cell1	P	100:0	50	1.3×10^{-6}	5.4	3500 ^d	42
Cell2	P	100:0	25	1.1×10^{-6}	5.2	3000 ^d	41
Cell3	P	75:25	25	8.9×10^{-7}	4.9	1900	51
Cell4	P	50:50	25	5.1×10^{-7}	4.9	1400	75
Cell5	P	25:75	25	3.5×10^{-7}	4.8	800	77
Cell6	P	10:90	25	1.7×10^{-7}	4.6	220	81
Cell7	P	0:100	25	0.4×10^{-7}	4.7	50	82
Cell8	P	0:100	50	4.4×10^{-7}	4.7	240	80
Cell9	T	50:50	25	1.2×10^{-7}	5.2	300	76
Cell10	T	100:0	25	7.7×10^{-7}	4.8	2600 ^d	42
Cell11	T	0:100	25	0.7×10^{-8}	4.6	30	82

^aP: planar alignment, T: twist alignment.

^bMBBA:EBBA (with error ± 2 wt. %).

^cValues at a fixed temperature $T = 35^{\circ}\text{C}$.

^dEstimated values where V_{WD} diverges.

^eTransition temperature T_c from the nematic to isotropic state, which was determined by the disappearance of EC.

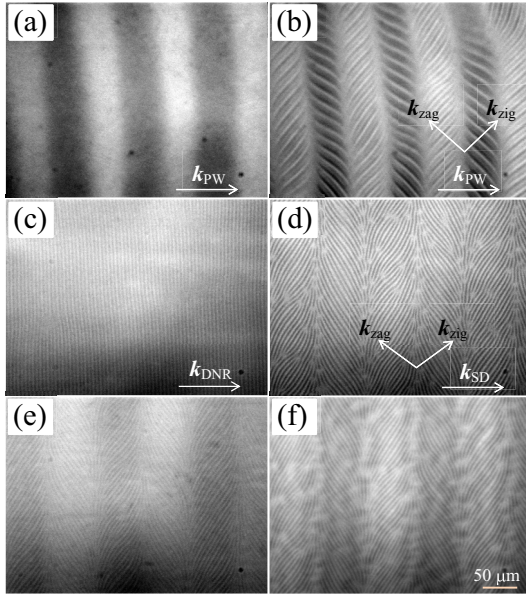


FIG. 2. Typical patterns of high-frequency ac-driven electroconvection (EC) observed in planarly aligned cells ($d = 25 \mu\text{m}$ and $T = 35^\circ\text{C}$); (a) prewavy (PW) at $V = 72 \text{ V}$ and $f = 2500 \text{ Hz}$, (b) defect-free chevron (DFC) at $V = 94 \text{ V}$ and $f = 2500 \text{ Hz}$, (c) dielectric normal rolls (DNRs) at $V = 59 \text{ V}$ and $f = 250 \text{ Hz}$, and (d) dielectric chevrons (DCV1) at $V = 60 \text{ V}$ and $f = 250 \text{ Hz}$; (e) and (f) were obtained from (d) under different optical conditions. In the crossed Nicol condition with a quarter-wave plate (PQA), (a), (b), and (e) were obtained, and (f) in the parallel Nicol with the same plate (PQP); (c) and (d) were obtained in a single polarizer (P). (a) and (b) were observed in Cell2 (MBBA), and (c)–(f) were observed in Cell7 (EBBA); note f_c for Cell2 and Cell7 in Table I. Of note, wide striped domains (SDs) that are parallel to DNRs ($k_{\text{SD}} // k_{\text{DNR}}$) in (e) are optically inverted in (f). The SDs and PW domains in the xy plane are characterized by the clockwise- and counterclockwise-twisting of the director field along the z axis.

the initial director \mathbf{n}_0 (i.e., $k_{\text{PW}} // \mathbf{n}_0 // \hat{x}$). Then, the WD is split by zig and zag rolls on PW; the wave vectors $k_{\text{zig}} (k_x k_y > 0)$ and $k_{\text{zag}} (k_x k_y < 0)$ represent the corresponding clockwise- and counterclockwise-twisted domains; i.e., $k_{\text{zig,zag}} // \mathbf{n}_{xy} (z = d/2)$ in the corresponding domains [25], as $k_{\text{WD}} // \mathbf{n}_0$ in the normal WD [2,5]; here, \mathbf{n}_{xy} indicates an in-plane director of \mathbf{n} , which is projected in the xy plane ($z = d/2$). On the other hand, the DNR with $k_{\text{DNR}} // \mathbf{n}_0$ [Fig. 2(c)] for $f > f_c$ evolves into a DCV [Fig. 2(d)] with an increase in V [16]; the DCV has k_{SD} for the SD and k_{zig} and k_{zag} , which is similar to the case of DFC [Fig. 2(b)]. Moreover, the DCV has clockwise- and counterclockwise-twisted domains in the PQA [Fig. 2(e)] or PQP [Fig. 2(f)] [17]; of note, their domains are optically inverted in both optical conditions and very similar to those of PW [Fig. 2(b)]. In addition, the wavelengths of PW and SD are nearly equivalent at a fixed $d (= 25 \mu\text{m})$ (i.e., $\lambda_{\text{PW}} = 2\pi/k_{\text{PW}} \sim 4d$ and $\lambda_{\text{SD}} = 2\pi/k_{\text{SD}} \sim 4d$), although their weak frequency dependence is not considered here.

We are interested in knowing what similar domains originate from; in other words, we need to determine whether PW has the same instability in a DCV as that in a DFC. The

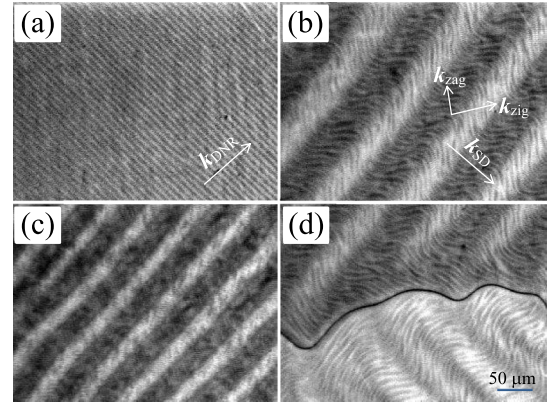


FIG. 3. Unique pattern evolution of EC ($f = 2000 \text{ Hz}$) observed in a twisted-aligned cell (Cell9), which is set under the PQA condition ($d = 25 \mu\text{m}$ and $T = 35^\circ\text{C}$): (a) DNR ($V = 155 \text{ V}$) \rightarrow (b) DCV-like pattern (DCV2) ($V = 158 \text{ V}$) \rightarrow (c) developed DCV-like pattern ($V = 168 \text{ V}$). (d) DCV2 was often observed in separated domains where it showed different SD directions that are perpendicular to each other ($V = 158 \text{ V}$). Of note, the SD in (b) appears in a perpendicular direction with respect to the DNR in (a) (i.e., $k_{\text{SD}} \perp k_{\text{DNR}}$); this considerably differs from that of the typical DCV1 in planarly aligned cells [Fig. 2(d)]. The wide SD in (b)–(d) was also optically inverted, which is similar to typical DCV1 [Figs. 2(e) and 2(f)]. In fact, $k_{\text{SD}} \equiv k_{\text{PW}}$ [observed in Fig. 2(a)]; see the text.

following two possibilities can be considered for the origin of an SD: one is the PW as a background pattern, such as that in a DFC [Fig. 2(b)], and the other is a defect-mediated secondary instability providing twisted director modulations [18]. The periodically ordered defects in the DCV exist for the latter, which is critically different from the DFC without defects. The theoretical and experimental results strongly support the latter possibility for the DCV [16,18]. However, the former should not be neglected because PW can still exist below the DCV ($V_{\text{PW}} < V_{\text{DCV}}$) in the high-frequency regime ($f > f_c$); it can form a DCV, which provides optical similarity resulting from the twisted directors.

Next, to determine the origin of an SD in a DCV, we examine the pattern formation for $f > f_c$ by using a T-type cell (Cell9) [8]. Figure 3(a) shows a DNR evolving into a unique pattern [Fig. 3(b)] through an increase in V . Clearly, the DCV-like pattern in the T-type [Fig. 3(b)] considerably differs from a typical DCV in the P-type [Fig. 2(d)]. The SD is formed perpendicular to the DNRs ($k_{\text{SD}} \perp k_{\text{DNR}}$), and thus, considerably differs from that of a typical DCV parallel to the rolls ($k_{\text{SD}} // k_{\text{DNR}}$) [Fig. 2(d)]. The wavy modulations of the rolls in Fig. 3(b) gradually occur with the SD's appearance; however, the periodic ordering of defects observed in the typical DCV [Fig. 2(d)] is not remarkable near V_{DCV} . Consequently, the SD should be considered as a PW instability induced above the threshold V_{DNR} , independent of such a defect-mediated secondary instability (i.e., $k_{\text{SD}} \equiv k_{\text{PW}}$). Therefore, this observation can support the former possibility that PW can arise as a background pattern of DCV formation in the P-type cell ($k_{\text{SD}} // k_{\text{DNR}}$). If the PW instability exists below the threshold V_{DCV} , the formation of a DCV that is independent of PW is unnatural (i.e., a pure defect-mediated DCV without any relation to PW). For a PW-originated DCV, the generation of defects

appears to be natural in the slightly developed normal rolls, as can be observed in fluctuating WD following the normal WD ($f < f_c$) through increasing V [20]. Moreover, the periodic ordering of defects can be formed, as observed in the defect lattice [26], with the aid of another twisting mode, known as an abnormal roll instability [27,28]. In the formation process of chevrons, PW may arise after a DNR (i.e., $V_{PW} > V_{DNR}$) for a DCV ($f > f_c$), as it does before a WD (i.e., $V_{PW} < V_{WD}$) for a DFC ($f < f_c$). Furthermore, the wavelength λ_{SD} decreases with a further increase in V [Fig. 3(c)]; this is similar to the case of a pure PW [29], and we also observe such behavior in a typical DCV (see below). In addition, for a T-type cell, an SD frequently appears in two completely separated domains (with clockwise- and counterclockwise-twisted director fields) through a sudden increase in V , as shown in Fig. 3(d); the upper and lower domains show SDs perpendicular and parallel to the DNR (i.e., $k_{SD} \perp k_{DNR}$ and $k_{SD} // k_{DNR}$), respectively. Evidently, two types of chevrons exist in the dielectric regime ($f > f_c$); therefore, we call them DNR-developed (or defect-mediated) DCV1 and PW-originated DCV2. Moreover, DCV2 is also observed in P-type cells (see below).

B. Threshold voltages as a function of frequency

We measure the threshold voltages of PW, DNR, DCV1, and DCV2 as a function of f . For example, Fig. 4(a) shows the threshold function $V_{PW}(f)$ of the pure PW at a different temperature T , which varies the electric conductivity $\sigma_{//,\perp}$ for EC [5]. The pure PW shows $\alpha_{PW} = 0.15 \pm 0.02$ in the power law, $V_{th} \propto f^\alpha$; this value is in a quantitative agreement with that in a systematic study conducted in Ref. [12], which uses several sample cells with different conductivities $\sigma_{//}$. On the other hand, the predicted $\alpha_{DNR} = 0.5$ for the DNR can be reproduced in Fig. 4(b) despite using the T-type cell (Cell9). In previous studies [3,4,8,12], only $\alpha_{DCV} = 0.5$ for DCV1 was reported because no stable DNR was observed (see below) [4,8,12,21]. Furthermore, Fig. 5 shows the power indices (i.e., α_{PW} , α_{DNR} , and α_{DCV}) as a function of T , which are determined by their f -dependent thresholds $V_{th} \propto f^\alpha$ (Fig. 4). Compared to the relatively robust values of $\alpha_{PW} = 0.15 \pm 0.02$, the values of α_{DNR} , α_{DCV1} , and α_{DCV2} ($= 0.48 \pm 0.05$) considerably deviate from the expected value $\alpha = 0.5$ [2,5,16,20]. In addition, α_{DNR} , α_{DCV1} , and α_{DCV2} appear to decrease with an increase in T , and α_{PW} decreases slightly [12]. In future studies, this tendency and deviation should be carefully considered in experiments and theory. However, the thresholds for DCV1 and DCV2 can be dealt with in the same category, independent of the cell type.

C. Possible scenarios for pattern formation and evolution in the dielectric regime

Let us recall the origin of the twisted director-modulated domains in DCVs (i.e., DCV1 and DCV2). Considering the two types of DCVs and the PW, there are three possible scenarios for DCV formation with an increase in V , as shown in Fig. 6; the slopes of the (solid, broken, and dotted) lines for the corresponding thresholds V_{th} (i.e., V_{DNR} , V_{DCV1} , and V_{PW}) indicate the power indices (i.e., α_{DNR} , α_{DCV1} , and α_{PW}) for the instabilities in the function of $V_{th} \propto f^\alpha$. (1) For $V_{PW} > V_{DCV1}$,

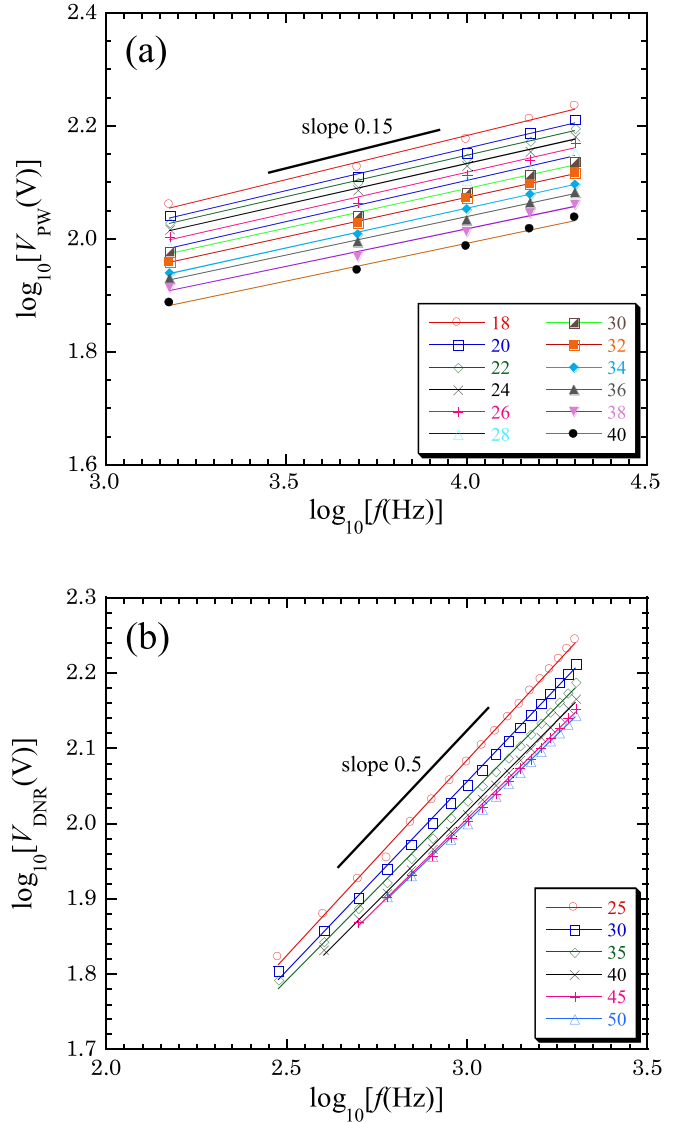


FIG. 4. Frequency dependence of the thresholds for pure PW (Cell2) (a) and DNR (Cell9) (b) with respect to different temperature T . The slopes of $V_{PW}(f)$ and $V_{DNR}(f)$ indicate the power indices, α_{PW} and α_{DNR} , of the relationship $V_{th} \propto f^\alpha$; they were calculated by the least-squares method. Notice the typical values ($\alpha_{PW} = 0.15$ and $\alpha_{DNR} = 0.5$) for both instabilities; see also Fig. 5.

DCV1 evolves from the DNR, independent of the PW, as shown in Fig. 6(a). This case has been frequently observed previously [12,16,17,20], not to mention the PW; however, there is a possibility of overlooking the PW in the single P condition, and the combined PW (at V_{PW}) may also be indistinguishable from DCV1 even under PQA and PQP conditions (owing to the equivalent director domains in both patterns) [29]. (2) For $V_{PW} < V_{DNR}$, DCV2 directly appears not via the (stable) DNR [4,8,21], because the PW exists as a background pattern before DCV2, as shown in Fig. 6(b). However, in many previous studies [4,8,21], the PW may not have been provided owing to the above-mentioned reason [29]. (3) For $V_{PW} > V_{DNR}$ (for $f < f^*$, see below), DCV2 arises at V_{PW} after the appearance of a DNR (and DCV1). If the voltage difference between V_{DCV1} and V_{PW} is small, DCV2 may not

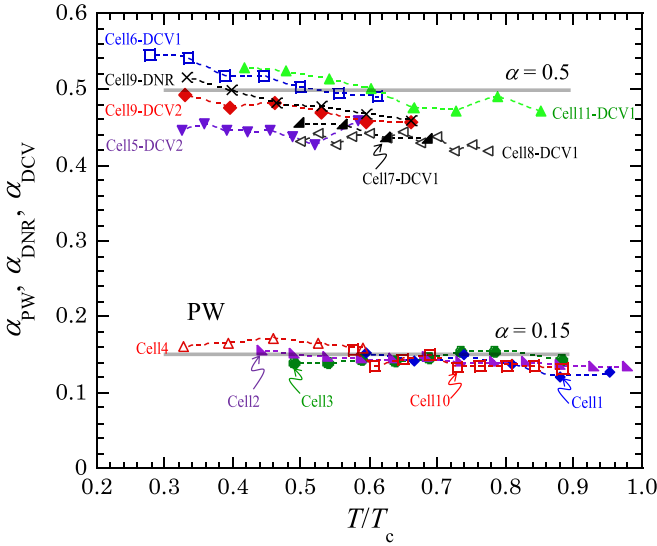


FIG. 5. Temperature-dependent power indices (α_{PW} , α_{DNR} , and α_{DCV}) determined by the frequency dependences of corresponding thresholds, as shown in Fig. 4. In particular, α_{PW} (≈ 0.15) for pure PW considerably differs from α_{DNR} , α_{DCV1} and α_{DCV2} around $\alpha = 0.5$. T_c indicates a transition temperature from NLC to the isotropic state for each cell; see Table I.

be distinguished from DCV1. Moreover, the pattern evolution can be changed above a certain frequency f^* , which is crossed by the threshold lines of both $V_{PW}(f)$ and $V_{DNR}(f)$. Note that due to unknown reasons, the slopes for DNR and DCV1 and DCV2 (i.e. the power indices) are slightly away from one another. Furthermore, the slope of the PW combined with DCV1 and DCV2 may differ from that of the pure PW, as seen in Fig. 6(c); it is because the PW above the DNR (and DCV1) threshold may be induced in different conditions such as the director field and flows, which are homogeneous and rest state for the pure PW below the DNR threshold. Thus, a transition from the DNR to (combined) PW (as a pattern of DCV2) for $f < f^*$ is changed by the other from (pure) PW to DCV2 for $f > f^*$, for which this pure PW acts as a background pattern of DCV2 ($V_{PW} < V_{DNR}$), as in case (2). In the experiment, the possibility of such a change in the pattern evolution is observed when the difference in the threshold voltages of both instabilities (i.e., $\Delta V = V_{DCV} - V_{DNR}$) decreases with an increase in f , as quantitatively described in Ref. [20]; if the DCV is independent of PW, ΔV does not depend on f , because $\alpha_{DNR} \approx \alpha_{DCV1} = 0.5$ [16]. However, in this study, it was not possible to obtain the direct observation of the entire patterns for the change in such transition scenarios, owing to the low optical resolutions at high voltages and the small difference in the two thresholds (see below).

To obtain direct evidence of the possible scenarios proposed in Fig. 6, the threshold voltages are measured as a function of f , as shown in Fig. 7. In particular, to obtain the possible scenarios, a set of sample cells with different rates of mixed NLCs (MBBA and EBBA) is prepared as described in Table I. The threshold functions shift to a high-frequency region with an increase in the rate of MBBA (at a fixed $T = 35^\circ\text{C}$); such a shift is very similar to that caused by conductivity in Ref. [12]. Moreover, the above-mentioned typical values

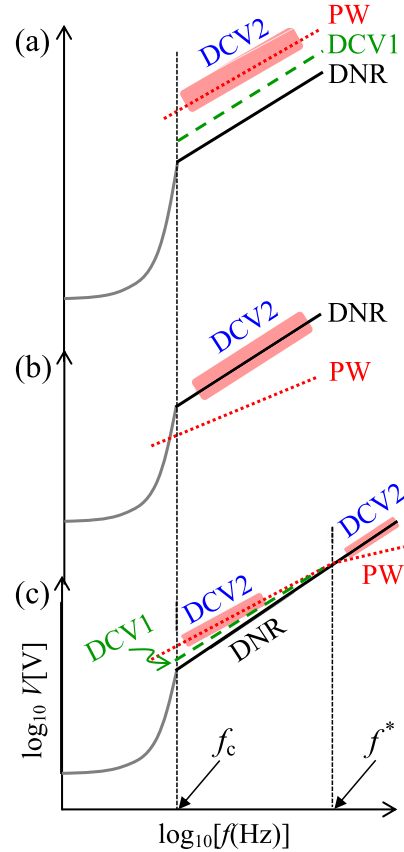


FIG. 6. Possible scenarios for pattern evolution in a high-frequency dielectric regime ($f > f_c$). (a) For $V_{PW} > V_{DCV1}$, a pattern transition (DNR \rightarrow DCV1) can be found with an increase in V ; at V_{PW} , DCV2 may still appear, but the slope of the threshold line and the spacing of wide domains may vary. Probably, PW instability cannot be perceived owing to the similar director domains in DCV1 and PW (Figs. 2, 7, and 8). The areas shadowed in red indicate that DCV2 appears at the PW threshold [(a) and $f < f^*$ in (c)] or DNR threshold [(b) and $f > f^*$ in (c)]. (b) For $V_{PW} < V_{DNR}$, a pattern transition (PW \rightarrow DCV2) cannot be determined by a (stable) DNR because pure PW exists as a background pattern (Figs. 7 and 9). (c) For $V_{PW} > V_{DNR}$ (or $V_{PW} < V_{DNR}$), two types of pattern evolutions [DNR \rightarrow (DCV1 \rightarrow)DCV2 for $f < f^*$ and PW \rightarrow DCV2 for $f > f^*$] can be determined; PW for $f < f^*$ and DNR for $f > f^*$ may be determined as DCV2 (i.e., the combination of DNR and PW); see also Figs. 3, 7, and 9. The slope (i.e., α_{PW}) of the PW for DCV2 may differ from that of the pure PW because of their occurrence conditions; see the text.

of α_{PW} , α_{DNR} , and α_{DCV} are reproduced. More importantly, the thresholds measured in Cell7, Cell4, and Cell6 exhibit the pattern evolutions shown in Figs. 6(a)–6(c), respectively. The behavior of the thresholds observed in Cell7 has been typically reported in many previous studies [12,16,17,20]. Of note, in Cell4, DCV2 appears instead of the DNR [Fig. 6(b)], owing to the occurrence of PW as a background pattern of DCV2 (Fig. 9); thus, DCV2 should be interpreted as a combination of PW and DNR [8,21]. Furthermore, in Cell6, the DNR disappears above a certain frequency [i.e., f^* in Fig. 6(c)] [20]; this confirms a change in the pattern evolution described in Fig. 6(c), although the direct observation of

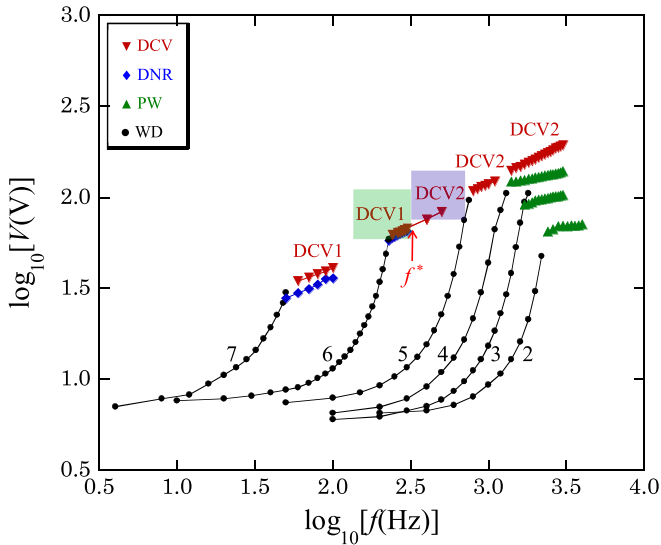


FIG. 7. Threshold voltages of instabilities (DCV1, DCV2, DNR, PW, and WD) at the fixed values of temperature and thickness ($T = 35^\circ\text{C}$ and $d = 25\ \mu\text{m}$); the number for each $V_{\text{th}}(f)$ indicates the corresponding cell in Table I. The frequency-dependent thresholds shift to the high-frequency region with an increase in the rate of MBBA to EBBA in the cells. Compare the thresholds for Cell7, Cell4, and Cell6 with those in Figs. 6(a)–6(c), respectively. No DCV was found in Cells 2 and 3 because of the high threshold voltage for high conductivity (Table I); see also Ref. [23].

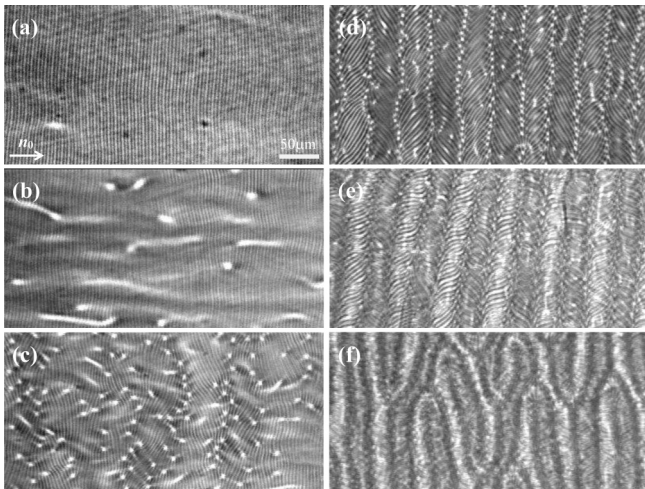


FIG. 8. Pattern evolution in Cell7 with low conductivity with an increase in voltage $V(f = 80\ \text{Hz}) = 36\ \text{V}$ (a), $38\ \text{V}$ (b), $40\ \text{V}$ (c), $42\ \text{V}$ (d), $50\ \text{V}$ (e), and $60\ \text{V}$ (f); see the pattern evolution to PW (i.e., DCV2) via DNR and DCV1 in Fig. 6(a), as well as the threshold $V_{\text{th}}(f)$ for Cell7 in Fig. 7. A DNR appears primarily (a), and defects in the DNR appear randomly (b) and they begin to be organized periodically (c), and eventually a DCV1 is completed (d). Above the DCV1 threshold, the DCV1 successively evolves into a complicated superstructure (f) via a transient pattern (e). Such a DNR-developed (or defect-mediated) DCV1 has been typically reported in previous studies, which should be distinguished from PW-originated DCV2 [Fig. 9(b)]. By comparing the new superstructure (f) with a similar structure [Fig. 9(f)], no considerable differences are observed except for the wave numbers.

the transition from PW to DCV2 for $f > f^*$ is not obtained because of $V_{\text{PW}} \approx V_{\text{DCV2}}$. However, DCV2 is clearly observed for $f > f^*$ [20]. Similarly, DCV2 primarily appears at V_{th} in Cell5, which is formed by a combination of PW and DNR for $V_{\text{PW}} \approx V_{\text{DNR}}$. The transition from PW to DCV2 is observed for $V_{\text{PW}} \ll V_{\text{DCV2}}$ in Cell4 (see below).

D. Pattern evolutions of PW-originated and defect-mediated chevrons

As shown in Figs. 6 and 7, PW can arise below and above the DNR threshold, owing to the physical properties of NLCs (mainly, conductivity). To determine the difference in DCVs in the two cases [i.e., Figs. 6(a) and 6(b)], we observe the pattern evolutions in Cell7 and Cell4 (Fig. 7). Figure 8 exhibits a pattern evolution by increasing V (at a fixed $f = 80\ \text{Hz}$); see the threshold $V_{\text{th}}(f)$ for Cell7 in Fig. 7. The primary instability, which provides the DNR [Fig. 8(a)], is destabilized in the presence of defects [Fig. 8(b)], and then developed into a typical DCV1 [Fig. 8(d)] through the gradual ordering of defects [Fig. 8(c)] [16,17,20]. Moreover, a different superstructure with macroscopic defects [Fig. 8(f)] is observed after a more developed DCV [Fig. 8(e)] [20]. Finally, it evolves into a well-known dynamic scattering mode 2 (DSM2), which is not observed in Fig. 8 [20]. Here, although PW seems to appear in chevron patterns [Figs. 8(e) and 8(f)], as proposed in Fig. 6(a), we cannot confirm whether they have PW as a background pattern. However, the DCV pattern [Fig. 8(f)] is quite similar to the PW-originated one [Fig. 9(f)] (see below); usually, for $V \gg V_{\text{PW}}$, both are indistinguishable from each other in this study.

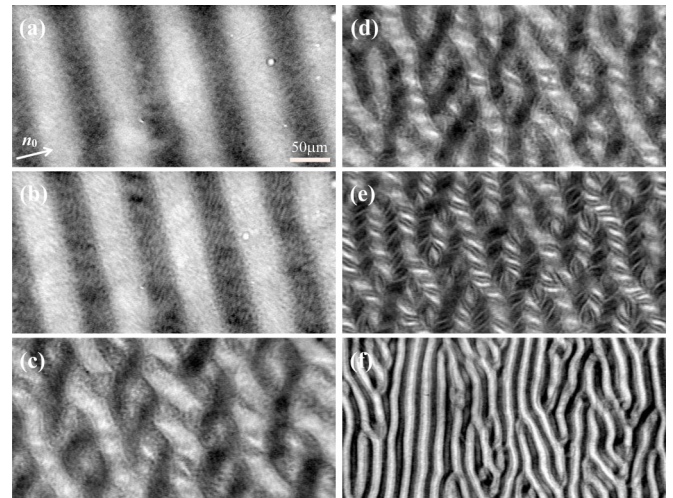


FIG. 9. Pattern evolution in Cell4 with high conductivity with an increase in voltage $V(f = 1600\ \text{Hz}) = 149\ \text{V}$ (a), $151\ \text{V}$ (b), $153\ \text{V}$ (c), $155\ \text{V}$ (d), $157\ \text{V}$ (e), and $170\ \text{V}$ (f); see the pattern evolution to DCV2 in Fig. 6(b) and the threshold $V_{\text{th}}(f)$ for Cell4 in Fig. 7. A PW appears primarily (a) and a DCV2 is formed by combing with a DNR (b). Above the DCV2 threshold, the DCV2 experiences a new unknown instability (c) and successively evolves into a new structure (f) through increasing the wave number and hiding WD-like rolls [(d) and (e)]. Compare DCV2 (b) in this P-type cell with DCV2 [Fig. 3(b)] in the T-type cell. Of note, PW-originated DCV2 (b) can be differentiated from the defect-mediated DCV1 [Fig. 8(d)].

On the other hand, Fig. 9 shows a different pattern evolution in Cell4, with an increase in V (at a fixed $f = 1600$ Hz); see the threshold $V_{th}(f)$ for Cell4 in Fig. 7 and also Fig. 6(b). PW [Fig. 9(a)] first arises as a background pattern of DCV2; then, DCV2 [Fig. 9(b)] appears as a combination of PW and DNR [8,21]. The fine structure has short DNRs. In addition, we compare DCV2 [Fig. 9(b)] in this P-type cell with that observed in the T-type cell [Fig. 3(b)]; of note, the former and latter DCV2 are observed for $V_{PW} < V_{DNR}$ and $V_{PW} > V_{DNR}$, respectively. Moreover, a complicated structure [Fig. 9(c)] is observed and grows into knitlike patterns [Figs. 9(d) and 9(e)] [13]; finally, such a superstructure [Fig. 9(f)] is also observed, as shown in Fig. 8(f). However, the fine structures of DCV2 are not observed in Figs. 9(d)–9(f), owing to their low optical resolution. Usually, the superstructures [Figs. 8(f) and 9(f)] observed in two different routes of pattern evolutions are indistinguishable from each other, although their different wave numbers are determined by unknown properties of NLCs. Such pattern evolutions, including superstructures following the DCVs, are reported in this paper; in terms of the hierarchy of structures, they should be investigated in the future study. Most importantly, PW-originated DCV2 [Fig. 9(b)] can be clearly differentiated from the conventional defect-mediated DCV1 [Fig. 8(d)] [2–5,13,20].

IV. SUMMARY AND CONCLUSION

We observed a PW-originated DCV (DCV2) following the DNR in a T-type cell, which was distinguished from a typical defect-mediated DCV (DCV1) in a P-type cell. DCV2 is a combination of DNR and PW with wide clockwise- and counterclockwise-twisted domains that are perpendicular to the DNR rolls ($\mathbf{k}_{PW} \perp \mathbf{k}_{DNR}$). In particular, DCV2 provides crucial evidence that a DCV can be formed in the presence of PW. In other words, DCV2 may arise as a combination of DNR and PW with wide domains that are parallel to DNR rolls ($\mathbf{k}_{PW} // \mathbf{k}_{DNR}$) in a P-type cell. In this study, DCV2 was observed in P-type cells. Moreover, we examined the power indices (α_{PW} , α_{DNR} , α_{DCV1} , and α_{DCV2}) of the frequency-dependent thresholds of PW, DNR, DCV1, and DCV2 in the function of $V_{th} \propto f^\alpha$. By considering the power indices as well as the existence of PW as a background pattern of DCV2 (Fig. 6), the pattern formation and evolution in the dielectric regime of EC can be understood well, which may have been overlooked in previous studies; accordingly, three possible scenarios to DCVs were proposed. In particular, PW-originated DCV2 [Figs. 3(b) and 9(b)] has been successfully

differentiated from the defect-mediated DCV2 [Figs. 2(d) and 8(d)], which has been typically mentioned in previous studies. However, the mechanism of PW occurrence has not been clarified. Although a theoretical model has been proposed by considering the inertia term in the Navier-Stokes equation [5,22], a sufficient agreement with the experimental results has not been reached. For example, the wavelength ($\lambda_{iner} \sim d$) and power index ($\alpha_{iner} \sim 1$) of the inertia mode-induced director domains are considerably different from those ($\lambda_{PW} \sim 4d$ and $\alpha_{PW} \sim 0.15$) of pure PW [Figs. 2(a), 4(a), and 5].

In addition, four models can be considered for the formation mechanism of chevrons. (1) The defect-mediated model, proposed by Rossberg and Kramer [18], can successfully explain a defect-mediated chevron (DMC) ($f < f_c$) [9] and DCV1 ($f > f_c$), which is independent of PW. It is considered as a frame of a general reaction-diffusion model that generates a Turing pattern (i.e., chevrons with periodic defects) [16–18,30]. In this case, the topological charge density of defects and the in-plane rotation of the director for twisting modulation act as the activator and inhibitor, respectively [18]. (2) The mode-coupling models, proposed by Sakaguchi and Matsuda [19], exhibit DFC, DMC [9], and defect lattices [26] as well as DNR and DCVs by varying a stabilizing parameter for the director (e.g., magnetic field) and the anisotropic properties of EC systems (e.g., ε and σ). This numerical study, which considers the EC amplitude A and phase ϕ for the in-plane director \mathbf{C} , reproduces chevron patterns; however, it cannot explain the mechanism of DCVs beyond conventional competition effects owing to the attractive and repulsive torques between the wave vector \mathbf{k} and director \mathbf{C} . Thus, such PW-originated DCV2 cannot be understood. (3) The beating model developed by two dielectric roll modes (with k_{DNR1} and k_{DNR2}), proposed by Kai and Zimmermann [20], can explain the larger periodicity (i.e., $k_{SD} = |k_{DNR1} - k_{DNR2}|$) of the wide domains of DCV1 with smaller dielectric rolls. However, the periodic defect lines of DCV1 cannot be satisfactorily understood. (4) In this study, the PW-originated model was proposed, which did not disallow the defect-mediated model (1), which can provide a better understanding of the experimental results on chevron formation and pattern evolution in high-frequency EC.

ACKNOWLEDGMENT

This work was supported by JSPS KAKENHI Grant No. 15K05215.

-
- [1] M. C. Cross and P. C. Hohenberg, *Rev. Mod. Phys.* **65**, 851 (1993).
 - [2] N. Eber, P. Salamon, and A. Buka, *Liq. Cryst. Rev.* **4**, 101 (2016).
 - [3] Orsay Liquid Crystal Group, *Phys. Rev. Lett.* **25**, 1642 (1970).
 - [4] M. I. Barnik, L. M. Blinov, M. F. Grebenkin, and A. N. Trufanov, *Mol. Cryst. Liq. Cryst.* **37**, 47 (1976).
 - [5] L. M. Blinov and V. G. Chigrinov, *Electro-Optical Effects in Liquid Crystal Materials* (Springer, New York, 1994).
 - [6] R. Williams, *J. Chem. Phys.* **39**, 384 (1963).
 - [7] E. F. Carr and W. Helfrich, *J. Chem. Phys.* **51**, 4092 (1969).
 - [8] L. Nasta, A. Lupu, and M. Giurgea, *Mol. Cryst. Liq. Cryst.* **71**, 65 (1981).
 - [9] J.-H. Huh, Y. Hidaka, A. G. Rossberg, and S. Kai, *J. Phys. Rev. E* **61**, 2769 (2000).

- [10] J.-H. Huh, Y. Hidaka, Y. Yusuf, N. Eber, T. Toth-Katona, A. Buka, and S. Kai, *Mol. Cryst. Liq. Cryst.* **364**, 111 (2001).
- [11] J.-H. Huh, Y. Yusuf, Y. Hidaka, and S. Kai, *Phys. Rev. E* **66**, 031705 (2002).
- [12] A. N. Trufanov, L. M. Blinov, and M. I. Barnik, *Zh. Eksp. Teor. Fiz.* **78**, 622 (1980) [*Sov. Phys. JETP* **51**, 314 (1980)].
- [13] K. S. Krishnamurthy, P. Tadapatri, and P. Viswanath, *Soft Matter* **10**, 7316 (2014).
- [14] S. Tanaka, S. Dhara, B. K. Sadashiva, Y. Shimbo, Y. Takanishi, F. Araoka, K. Ishikawa, and H. Takezoe, *Phys. Rev. E* **77**, 041708 (2008).
- [15] B. Katranchev and M. Petrov, *Comp. Ren. Acad. Bulg. Sci.* **62**, 329 (2009).
- [16] M. Scheuring, L. Kramer, and J. Peinke, *Phys. Rev. E* **58**, 2018 (1998).
- [17] H. Amm, R. Stannarius, and A. G. Rossberg, *Physica D* **126**, 171 (1999).
- [18] A. G. Rossberg and L. Kramer, *Physica D* **115**, 19 (1998).
- [19] H. Sakaguchi and A. Matsuda, *Physica D* **238**, 1 (2009).
- [20] S. Kai and W. Zimmermann, *Prog. Theor. Phys. Supp.* **99**, 458 (1989).
- [21] P. Petrescu and M. Giurgea, *Phys. Lett. A* **59**, 41 (1976).
- [22] S. A. Pikin and V. G. Chigrinov, *Zh. Eksp. Teor. Fiz.* **78**, 246 (1980) [*Sov. Phys. JETP* **51**, 123 (1980)].
- [23] In experiment, the conductivity can be controlled by mixing a dopant (e.g., DMOAP), which is increased with the amount of a dopant [10]. In this study, since our pure MBBA (Cell1, Cell2, and Cell10) had sufficiently high conductivity as seen in Table I, the dielectric patterns (i.e., DNR, DCV1, and DCV2) could not be observed because of their thresholds much higher than the experimental limitations; see data of Cell1, Cell2, and Cell10 in Figs. 5 and 7. Therefore, in order to examine the dielectric patterns for low conductivity, we employed the mixing of EBBA with MBBA that can decrease the conductivity with the mixing rate; see Cell2–7 in Table I and Fig. 7.
- [24] J.-H. Huh and H. Osoguchi, *Phys. Rev. E* **101**, 062701 (2020).
- [25] C. G. Jhun, G. J. Choi, D. G. Ryu, J.-H. Huh, and J. S. Gwag, *Phys. Rev. E* **98**, 052704 (2018).
- [26] N. Oikawa, Y. Hidaka, and S. Kai, *Phys. Rev. E* **70**, 066204 (2004).
- [27] E. Plaut, W. Decker, A. G. Rossberg, L. Kramer, W. Pesch, A. Belaidi, and R. Ribotta, *Phys. Rev. Lett.* **79**, 2367 (1997).
- [28] J.-H. Huh, Y. Hidaka, and S. Kai, *J. Phys. Rev. E* **58**, 7355 (1998).
- [29] J.-H. Huh and N. Miyagawa (unpublished).
- [30] A. M. Turing, *Phil. Trans. R. Soc. B* **237**, 37 (1952).